Monomeric Sarcosine Oxidase: Role of Histidine 269 in Catalysis[†,‡]

Gouhua Zhao,[§] Hui Song,[§] Zhi-wei Chen,[||] F. Scott Mathews,[||] and Marilyn Schuman Jorns*[,§]

Department of Biochemistry, MCP Hahnemann School of Medicine, Philadelphia, Pennsylvania 19129, and Department of Biochemistry and Molecular Biophysics, Washington University School of Medicine, St. Louis, Missouri 63110

Received April 16, 2002; Revised Manuscript Received May 21, 2002

ABSTRACT: Conservative mutation of His269 (to Asn, Ala, or Gln) does not-significantly affect the expression of monomeric sarcosine oxidase (MSOX), covalent flavinylation, the physicochemical properties of bound FAD, or the overall protein structure. Turnover with sarcosine and the limiting rate of the reductive half-reaction with L-proline at pH 8.0 are, however, nearly 2 orders of magnitude slower than that with with wild-type MSOX. The crystal structure of the His269Asn complex with pyrrole-2-carboxylate shows that the pyrrole ring of the inhibitor is displaced as compared with wild-type MSOX. The His269 mutants all form charge-transfer complexes with pyrrole-2-carboxylate or methylthioacetate, but the charge-transfer bands are shifted to shorter wavelengths (higher energy) as compared with wild-type MSOX. Both wild-type MSOX and the His269Asn mutant bind the zwitterionic form of L-proline. The E_{ox}·L-proline complex formed with the His269Asn mutant or wild-type MSOX contains an ionizable group ($pK_a = 8.0$) that is required for conversion of the zwitterionic L-proline to the reactive anionic form, indicating that His269 is not the active-site base. We propose that the change in ligand orientation observed upon mutation of His269 results in a less than optimal overlap of the highest occupied orbital of the ligand with the lowest unoccupied orbital of the flavin. The postulated effect on orbital overlap may account for the increased energy of charge-transfer bands and the slower rates of electron transfer observed for mutant enzyme complexes with charge-transfer ligands and substrates, respectively.

Monomeric sarcosine oxidase (MSOX) is a flavoprotein that contains covalently bound FAD [8α-(S-cysteinyl)FAD] (*1*). The enzyme oxidizes sarcosine (*N*-methylglycine) and other secondary amino acids, such as L-proline. Sarcosine is a common soil metabolite and induces MSOX expression in various bacteria grown with sarcosine as sole source of carbon and energy (*2*). MSOX is a member of a family of enzymes that contain covalently bound flavin and catalyze similar oxidation reactions with amine substrates (*1*, *3*, *4*). The crystal structure of free MSOX from *Bacillus sp. B-0618* and complexes of the enzyme with various inhibitors have recently been determined (*5*, *6*).

The anaerobic half-reaction of wild-type MSOX with L-proline, a slow substrate, proceeds via a rapidly attained equilibrium (K_d) between free E and the E·S complex, followed by a practically irreversible flavin reduction step associated with a rate constant, k_{lim}, that converts E_{ox}·S to E_{red}·P. As described in the accompanying paper, the effect of pH on this reaction shows that the K_d for L-proline binding is pH-independent. This indicates that MSOX binds the zwitterionic form of L-proline, the predominant species in solution at neutral pH ($pK_a = 10.6$). Values for the limiting rate of reduction (k_{lim}) are, however, strongly pH-dependent and indicate that an ionizable group in the E_{ox}·L-proline complex ($pK_a = 8.02$) must be unprotonated for conversion to E_{red}·P. Charge transfer interaction with FAD as acceptor and substrate as donor is possible only with the anionic form of L-proline. The ionizable group in the E·S complex is required for conversion of L-proline from the zwitterionic to the reactive anionic form, as judged by the independently determined pK_a for charge-transfer complex formation with wild-type MSOX ($pK_a = 7.94$).

MSOX-bound L-proline may exhibit a pK_a of 8.0 for conversion of the zwitterionic to the anionic form. Alternatively, conversion of the zwitterionic to the anionic form of bound L-proline may require proton transfer to a base in the E·S complex with a pK_a of 8.0. His269 or Tyr317 appear to be suitably positioned to act as an active-site base, as judged by the crystal structure of the MSOX complex with various inhibitors, including pyrrole-2-carboxylate (PCA) (see Figure 7). In the MSOX·PCA complex, ND1 of His 269 is located 3.60 Å away from the atom corresponding to the methyl group of sarcosine and 4.17 A from the atom corresponding to the amino nitrogen of sarcosine. The corresponding distances for the phenolic oxygen of Tyr317 are 3.54 and 4.58 Å, respectively.

[†] This work was supported in part by Grants GM 31704 (M.S.J.) and GM31611 (F.S.M.) from the National Institutes of Health.

[‡] Crystallographic coordinates have been deposited in the Protein Data Bank under the file names 1L9C (His269AsnMSOX), 1L9D (His269AsnMSOX·PCA complex), and 1L9E (wtMSOX·imidazole complex).

* Corresponding author. Phone: (215) 762-7495 FAX: (215) 762-4452. E-mail: marilynjorns@drexel.edu.

[§] MCP Hahnemann School of Medicine.

[||] Washington University School of Medicine.

[1] Abbreviations: MSOX, monomeric sarcosine oxidase; FAD, flavin adenine dinucleotide; PCA, pyrrole-2-carboxylate; MTA, methylthioacetate, EDTA, ethylenediaminetetraacetic acid; MSOX·imidazole complex (MSOX·IMD).

[2] The definitions of R_{merge}, R, and R_{free} are given in the legend to Table 2.

[3] Trickey, P., Chen, Z.-w., Jorns, M. S., and Mathews, F. S. Unpublished results.

10.1021/bi020286f CCC: $22.00
Published on Web 07/13/2002

Table 1: PCR Primers Used to Generate Mutations by the Overlap Extension Method[a]

	left-half primary reaction		right-half primary reaction	
mutation	name	sequence	name	sequence
His269Ala	START-R1	5′-ATGACCATGATTACGCCAAGC-3′	H269A#3	5′-GGATAT**gcc**ACGTTCGGGCA-3′
	H269A#2	5′-TGCCCGAACGT**ggc**ATATCC-3′	END-R4	5′-TTAAGTTGGGTAACGCCAGG-3′
His269Asn	START-R1	5′-ATGACCATGATTACGCCAAGC-3′	H269N#3	5′-GGATAT**aAc**ACGTTCGGGCA-3′
	H269N#2	5′-TGCCCGAACGT**gTt**ATATCC-3′	END-R4	5′-TTAAGTTGGGTAACGCCAGG-3′
His269Gln	START-R1	5′-ATGACCATGATTACGCCAAGC-3′	H269Q#3	5 -GGATAT**CAg**ACGTTCGGGGAG-3′
	H269Q#2	5 -TGCCCGAACGT**cTG**ATATCC-3′	END-R4	5′-TTAAGTTGGGTAACGCCAGG-3′

[a] Codon 269 is shown in bold, and mutagenic sites are indicated by lowercase letters.

In this paper, we characterize mutants with conservative substitutions (Asn, Ala, Gln) at His269. The reductive half-reaction with L-proline and turnover with sarcosine are decreased by about 2 orders of magnitude upon mutation of His269, indicating the importance of this residue in catalysis. His269 is not the ionizable group in the E·S complex formed with L-proline. Instead, His269 appears to be important in optimizing the orientation of bound substrate with respect to electron transfer to flavin.

EXPERIMENTAL PROCEDURES

Materials. Escherichia coli DH1 was obtained from the American Type Culture Collection (ATCC 33849). Plasmid pUC 119 was from Worthington Biochemical Corporation. All primers were synthesized by Ransom Hill Bioscience. The QiaQuick gel extraction kit, QiaQuick PCR purification kit, QiaPrep spin miniprep kit, Qiagen midiprep kit, and Taq PCR core kit were from Qiagen. *Pfu* DNA polymerase was purchased from Stratagene. dNTPs were from Pharmacia. T4 DNA ligase was obtained from New England Biolabs or Invitrogen. The TA cloning kit and One Shot *E. coli* competent cells (INVαF′) were from Invitrogen. All restriction enzymes were purchased from New England Biolabs. IPTG was obtained from Sigma. X-gal was from USB. Purified xanthine oxidase was a generous gift from Dr. Russ Hille (Ohio State University).

PCR. Reactions were performed using *Pfu* DNA polymerase and a Hybaid Touchdown Thermocycler with the following cycle settings: step 1, 94 °C for 3 min; step 2, 30 cycles of 94 °C for 40 s, 52 °C for 1 min, and 72 °C for 3 min; step 3, 72 °C for 30 min. PCR products and other DNA fragments were purified by agarose gel (1.2%) electrophoresis and recovered using the Qiaquick gel extraction kit.

Mutagenesis. Site-directed mutations were generated using PCR and the overlap extension method described by Ho et al. (*7*) with plasmid pMAW (*1*) as the template. For each mutant (His269Ala, His269Asn, His269Gln), left- and right-hand reaction fragments were created using the primers indicated in Table 1. These fragments were combined with primers START-RI and END-R4 to generate the secondary PCR products which correspond to the entire mutant gene, flanked near the 5′ and 3′ ends with unique *Pst*I and *Eco*RI restriction sites, respectively.

The secondary PCR products were treated with *Taq* polymerase and dNTP to add a single, 3′-A overhang to each end of the PCR product. The reaction was conducted using the Hybaid Touchdown Thermocycler as described above, except that the number of cycles in Step 2 was reduced to 3. The treated DNA fragments were purified with the QiaQuick PCR purification kit and then ligated with the linear vector, pCR2.1 (Invitrogen). The resulting plasmids were used to transform competent *E. coli* cells (INVαF′). The transformed cells were screened by growth on plates containing kanamycin and X-gal. Five to 10 white colonies were selected for further screening by restriction analysis using *Pst*I *and Eco*RI. The desired PstI-EcoRI restriction fragment containing the mutant MSOX gene was then subcloned between the *Pst*I *and Eco*RI sites of plasmid pUC119. The newly formed plasmids were used to transform *E. coli* DH1 cells to carbenicillin resistance. Plasmids from several colonies were initially screened by restriction analysis and then sequenced across the entire insert. Sequencing was conducted by Nucleic Acid/Protein Research Core Facility (NAPCORE) at the Children's Hospital of Philadelphia.

Purification of MSOX. Wild-type enzyme and various His269 mutants were purified as previously described (*1*). During enzyme purification, MSOX activity was measured using the Nash assay, and the protein was determined using the Bio-Rad micro protein assay (*1*).

Spectral Studies. Absorption spectra were recorded using a Perkin-Elmer Lambda 2S spectrometer. All extinction coefficients were determined at pH 8.0 as previously described (*1*).

Spectral titrations with methylthioacetate (MTA), pyrrole-2-carboxylate (PCA), or imidazole were conducted at 25 °C in 50 mM potassium phosphate buffer, pH 8.0. All spectra are corrected for dilution. For comparison of the spectral perturbations observed with different ligands, difference and absolute spectra were normalized to the same initial concentration of uncomplexed enzyme. Spectra were also normalized to 100% complex formation to compensate for differences in the maximal extent of complex formation observed in titrations with different ligands and/or enzyme preparations. The 100% complex spectra were calculated using the measured complex dissociation constants and spectral data obtained at the highest ligand concentration tested. These spectra were used to calculate the extinction coefficients for the complex at various wavelengths of interest. The positions of charge transfer bands were estimated from difference spectra. This approach was especially useful in the case where the charge-transfer band was not well-resolved in the absolute spectra owing to overlap with the high wavelength edge of the flavin absorption spectrum.

Anaerobic experiments were conducted using special cuvettes with two sidearms. The cuvettes were made anaerobic by purging with argon, as previously described (*5*).

Determination of Reduction Potentials. The redox potentials of wild-type and mutant (His 269Asn) forms of MSOX were determined in 50 mM potassium phosphate buffer, pH 8.0, containing 20 μM methyl viologen (mediator dye), 1

μM riboflavin, 60 μM EDTA, 300 μM xanthine, 20 μM toluylene blue (indicator dye) and a variable, catalytic amount of xanthine oxidase, following the spectrophotometric method described by Massey (*8*). MSOX and xanthine oxidase were placed in separate sidearms of an anaerobic cuvette. All other components were placed in the main compartment. The cuvette was made anaerobic as previously described (*5*). MSOX was tipped into the main compartment, and the spectrum of the enzyme solution was recorded. The reaction was started by adding xanthine oxidase. The concentration of the oxidized and reduced forms of toluylene blue were determined at 647 nm, a wavelength where the oxidized dye exhibits a absorption maximum but negligible absorbance is observed for the reduced dye or the oxidized or radical forms of MSOX. The oxidized and radical forms of MSOX were quantified on the basis of the absorbance at 391 nm (corrected for the contribution of the oxidized and reduced dye) using previously published extinction coefficients (E_{ox}, $\epsilon_{391} = 8940\ M^{-1}\ cm^{-1}$; E_{rad}, $\epsilon_{391} = 24\,900\ M^{-1}\ cm^{-1}$) (*5*). The oxidation/reduction potentials for the couple E_{ox}/E_{rad} (E_1) with wild-type or mutant forms of MSOX were determined as previously described (*8*) using the midpoint potential of toluylene blue, calculated at pH 8.0 ($E_m = 81.3$ mV, pH 8.0, $n = 2$) (*9*).

Steady-State Kinetics. Studies were conducted by monitoring hydrogen peroxide formation using a horseradish peroxidase coupled assay. Reactions were performed at 25 °C in 100 mM potassium phosphate buffer, pH 8.0, containing amino acid, oxygen, 320 μM *o*-dianisidine, 1.8 U horseradish peroxidase, and the His269Asn mutant in a total volume of 350 μL. Formation of oxidized *o*-dianisidine was monitored by the increase in absorbance at 460 nm ($\epsilon_{460} = 6765\ M^{-1}\ cm^{-1}$). Assays were conducted using a special cuvette (Spectrocell) with a screw-cap equipped with a Teflon-silicone membrane. The oxygen concentration was varied by equilibration of reaction mixtures containing all components except the two enzymes with various oxygen/nitrogen gas mixtures, as previously described (*10*). Horseradish peroxidase was injected into the sealed cuvette using a gastight Hamilton syringe. After a 2 min incubation at 25 °C, the reaction was initiated by injecting an aliquot of the His269Asn mutant, as previously described (*10*).

Data Analysis. Data were fit to eqs 1−4 using the curve fit function in Sigma Plot (Jandel Corporation). Equation 1 was used for the following:

$$Y = \frac{AX}{X + K} \quad (1)$$

$$Y = \frac{AH^+ + BK_a}{H^+ + K_a} \quad (2)$$

$$V = \frac{V_{max}AB}{K_aK_b + K_bA + AB} \quad (3)$$

$$\log k_{lim} = \log(C)/(1 + [H^+]/K_{a1} + K_{a2}/[H^+]) \quad (4)$$

(a) analysis of spectrophotometric titration data for complex formation between mutant and wild-type forms of MSOX and various ligands, where Y and A are the observed and maximal absorbance change at the wavelength selected for analysis, respectively, X is the concentration of the varied ligand, and K is the complex dissociation constant; (b) analysis of the apparent first-order rate of enzyme reduction by L-proline (k_{obs}) as a function of the substrate concentration, where Y and A are k_{obs} and k_{lim}, respectively, X is the L-proline concentration, and K is the apparent dissociation constant of the E·S complex. Equation 2 was used to fit the effect of pH on the absorption spectrum of (a) the uncomplexed His269Asn mutant ($\lambda_{analysis} = 352$ nm) and (b) the complex of the His269Asn mutant with L-proline ($\lambda_{analysis} = 502$ nm). Y is the observed absorbance or absorbance difference at the indicated analysis wavelength at a given pH value. A and B are the calculated absorbance or absorbance difference at this wavelength at low and high pH values, respectively. Equation 3 was used to fit the steady-state kinetic data obtained with the His269Asn mutant (E) at various concentrations of sarcosine and oxygen. K_a and K_b are the dissociation constants of oxygen and sarcosine from the E·oxygen and E·oxygen·sarcosine complexes, respectively. Equation 4 was used to fit the reductive half-reaction kinetics with the His269Asn mutant and L-proline as a function of pH. K_{a1} is the ionization constant of a group in the E·S complex that must be unprotonated for enzyme reduction to occur, and K_{a2} is the ionization constant of a group in the E·S complex that must be protonated for enzyme reduction to occur.

Crystallization and Data Collection. Crystals of MSOX mutants and ligand complexes were grown by the sitting drop method as described previously (*6*). Equal volumes of 5 μL each of protein solution (7 mg/mL in 20 mM Tris-HCl, pH 8.0) and reservoir solution (1.9−2.1 M Na/K phosphate buffer, pH 7.0) were mixed and allowed to equilibrate. The crystals of the wild-type MSOX·imidazole complex (MSOX·IMD) were obtained by co-crystallization with 500 mM imidazole at pH 7.0, while the crystals of the His269Asn·PCA complexwere obtained by soaking in saturated PCA for 35 min at pH 7.0.

X-ray data were recorded from a single-crystal each of His269Asn and the His269Asn·PCA complex at 100° K on a Rigaku R-axis II image plate detector and from a single crystal of the MSOX·IMD complex at 298° K on a Rigaku R-axis IV detector. For the *R*-axis II data a graphite-monochromatized X-ray beam and for the *R*-axis IV data a Ni-filtered, mirror-focused X-ray beam were used, both obtained from a Rigaku RU200 X-ray generator operated at 5 kW power. The crystals were monoclinic, space group $P2_1$, with unit cell parameters $a = 72.71$ Å, $b = 69.25$ Å, $c = 73.32$ Å ,and $\beta = 94.25°$ for His269Asn, $a = 71.41$ Å, $b = 69.77$ Å, $c = 73.17$ Å, and $\beta = 92.22°$ for the His269Asn·PCA complex, and $a = 73.08$ Å, $b = 70.64$ Å, $c = 74.30$ Å, and $\beta = 93.78°$ for the MSOX·IMD complex. The crystals all contained two protein molecules per asymmetric unit. Spot integration and data scaling were carried out using HKL (*11*). The data were generally 88−90% complete and scaled to the outer resolution limits (1.95−1.85 Å) with R_{merge}^2 between 0.056 and 0.072. The data collection statistics are summarized in Table 2.

Structure Determination and Refinement. The initial coordinates of the His269Asn·PCA complex were obtained by molecular replacement (MR) with AMORE (*12*) since the β angle changed somewhat after soaking the crystal. The structures of His269Asn and the MSOX·IMD complex could

Table 2: Data Collection and Structure Determination of His269Asn, the His269Asn·PCA Complex, and the Wild-Type(wt) MSOX·IMD Complex

	His269Asn	His269Asn·PCA	wtMSOX·IMD
reagent (concentrated)	−	PCA (saturated)	IMD (500 mM)
data collection			
resolution (Å)	30−1.9	30−1.95	30−1.85
no. of reflections	50561	47553	57602
completeness (all/outer 0.05 Å shell, %)	87.7/52.5	90.4/50.8	89.5/57.7
R_{merge}[a] (all/outer)	0.066/0.192	0.056/0.250	0.072/0.280
$\langle 1\rangle/\sigma$[b] (all/outer)	13.7/3.1	22.1/3.4	14.2/3.0
redundancy (all/outer 0.05 Å shell)	2.9/1.9	4.5/2.0	2.9/1.7
refinement			
R[c] (all/outer 0.05 Å shell)	0.171/0.243	0.184/0.254	0.168/0.251
R_{free}[d] (all/outer 0.05 Å shell)	0.216/0.291	0.228/0.288	0.195/0.262
no. protein atoms (non-H)[e]	6014	6014	6018
$\langle B\rangle$ (Å^2)	16.2	22.4	23.2
no. of alternate conformers	4	4	10
no. FAD atoms (non-H)[e]	106	106	106
$\langle B\rangle$ (Å^2)	11.0	15.4	14.1
no. of chloride ions[e]	2	2	2
$\langle B\rangle$ (Å^2)	12.2	17.1	16.1
no. of PO_4^{3-} ions	1	−	−
$\langle B\rangle$ (Å^2)	41.9	−	−
no. of ligand atoms (non-H)[e]	−	16	10
$\langle B\rangle$ (Å^2)	−	44.3	21.0
no. of solvent molecules[e]	1065	730	457
$\langle B\rangle$ (Å^2)	28.4	32.0	36.2
RMSD			
bonds (Å)	0.005	0.006	0.005
angles (deg)	1.50	1.50	1.40
ΔB (main-main, Å^2)	1.6	2.0	2.1
ΔB (main-side, Å^2)	2.0	2.4	2.6
ΔB (side-side, Å^2)	2.7	3.3	3.7

[a] $R_{merge} = \sum_h\sum_i I(h) - I_i(h)/\sum_h\sum_i I_i(h)$, where $I_i(h)$ and $I(h)$ are the ith and mean measurements of reflection h. [b] $I/\sum(I)$ is the average signal-to-noise ratio for merged reflection intensities. [c] $R = \sum_h(\text{Fo}-\text{Fc})/\sum_h$ Fo, where Fo and Fc are the observed and calculated structure factor amplitudes of reflection h. [d] R_{free} is the test reflection data set, about 10% selected randomly for cross validation during crystallographic refinement (*14*). [e] Per asymmetric unit which contains two molecules of MSOX.

be refined directly since no change in β had occurred. In both cases, the coordinates used were of an isomorphous complex of native MSOX with 2-furoate which was determined at 1.3 Å resolution[3], but with all ligands, solvent molecules, and alternate conformers omitted as the starting model.

The refinement and electron density map calculations were carried out using CNS (*13*), and 10% of the reflections were selected randomly and set aside as a test set for cross validation (*14*). Reflections from ∞ to the diffraction limit recorded for each data set (1.95 to 1.85 Å resolution, see Table 2) were included in the refinements, and a bulk solvent correction was applied (*15*).

Coordinates for the ligands bound at the active site were obtained from the Cambridge Structure Database (*16*). Noncrystallographic symmetry (NCS) restraints were applied to the two protein molecules in the asymmetric unit during refinement (with NCS weights set to 300 for both main and side chain atoms) except for two short polypeptide segments plus four side chains, all near the protein surface and which consistently differed from each other in the two subunits.

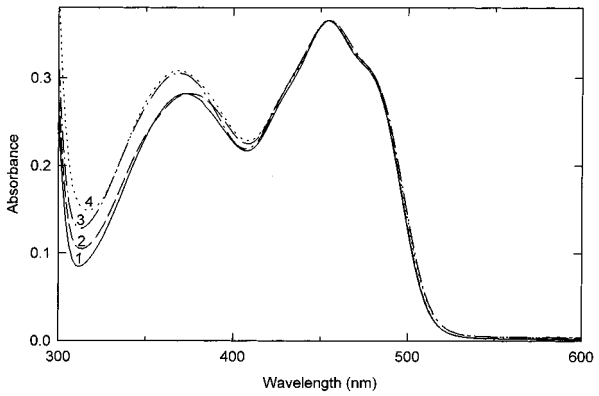

FIGURE 1: Comparison of visible absorption spectra of various His269 mutants and wild-type MSOX. Curve 1 (solid line) is the spectrum of wild-type MSOX. Curve 2 (dashed line) is the spectrum of the His269Asn mutant. Curve 3 (dashed−dotted line) is the spectrum of the His269Ala mutant. Curve 4 (dotted line) is the spectrum of the His269Gln mutant. Spectra were recorded in 50 mM potassium phosphate buffer, pH 8.0, at 25 °C and are normalized at 454 nm.

The differences between *B*-factors for bonded atoms were restrained using target standard deviations of 1.5 Å^2 for main chain and 2.0 Å^2 for side chain atoms, and reflections with $\sigma(I) < 0.0$ were omitted. Model building and analysis of the structures were carried out on a Silicon Graphics workstation using Turbo-Frodo (*17*). Four side chains in each of His269Asn and the His269Asn·PCA complexes and 10 side chains, including a loop region near the active site consisting of residue 55 to residue 61 of subunit A in the imidazole complex, were modeled in two alternate conformations. Several cycles of positional and temperature factor refinement, followed by interactive model building and automatic solvent placement with manual examination, were carried out. This procedure utilized electron density difference maps calculated with Fourier coefficients (2Fo−Fc) and (Fo−Fc), where Fo and Fc are the observed and calculated structure factors, respectively.

The quality of the refined structures and the resulting electron density maps of all three structures is high (Table 2). Agreement factors R and R_{free}[2] ranged from 0.168 to 0.184 and 0.195 to 0.228, respectively, with RMSD in bond length and angles of 0.005−0.006 Å and 1.40−1.50°, respectively. Between 457 and 1065 water molecules are included in the structures, and each protein molecule contains one bound chloride ion. The Ramachandran plot (*18*, *19*) for each crystal structure shows that one residue lies in a sterically disallowed region in each molecule of the asymmetric unit, Asp47. This residue which is located in a coil between the flavin binding and catalytic domains and its side chain is oriented differently in the two NCS-related molecules. The final refinement statistics are shown in Table 2.

RESULTS

General Properties of Various His269 Mutants. Mutation of His269 to Ala, Asn, or Gln does not significantly affect expression of MSOX. The mutant proteins could all be purified to apparent homogeneity, as judged by SDS−PAGE, using the same procedure developed for wild-type MSOX. The visible absorption spectrum of the His269Asn mutant (Figure 1, curve 2) at pH 8.0 virtually superimposes with that observed with wild-type enzyme (Figure 1, curve 1).

Table 3: Catalytic and Spectral Properties of Various His269 MSOX Mutants[a]

enzyme	specific activity	A_{280}/A_{454}	ϵ_{454} (mM^{-1} cm^{-1})
wild type	49	5.7	13.1[b]
His269Ala	2.1	6.2	13.2
His269Asn	1.7	5.6	13.5
His269Gln	1.5	6.8	13.6

[a] The activity and spectral ratio data for wild-type enzyme and the His269Asn mutant are averages of results obtained with two preparations. The His269Ala and His269Gln mutants were purified once. A unit of MSOX activity is defined as the formation of 1 μmol of formaldehyde/min at 37 °C with sarcosine as substrate (*1*). [b] A value of 12.2 mM^{-1} M^{-1} was previously reported (*1*).

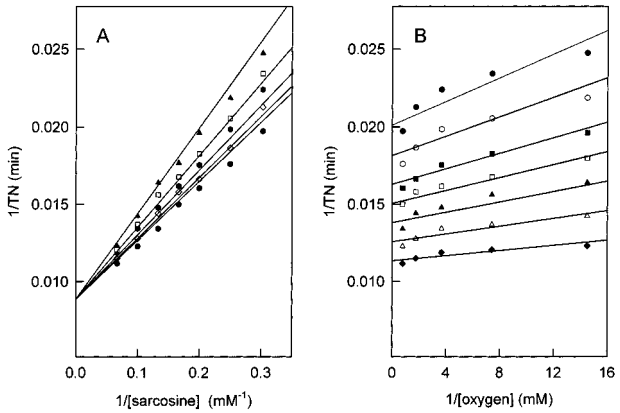

FIGURE 2: Steady-state kinetic data for the His269Asn mutant with sarcosine as substrate in 100 mM potassium phosphate buffer, pH 8.0, at 25 °C. The double reciprocal plots of TN vs sarcosine concentration (panel A) were obtained at various oxygen concentrations [0.069 (filled triangle) 0.135 (open square), 0.273 (filled hexagon) 0.566 (open diamond), and 1.279 mM (black circle)]. The double reciprocal plots of TN vs oxygen concentration (panel B) were obtained at various sarcosine concentrations [3.3 (filled circle), 4.0 (open circle), 5.0 (filled square), 6.0 (open square), 7.5 (filled triangle), 10 (open triangle), and 15 mM (filled diamond)]. The lines correspond to fits of the data to an equation for a rapid equilibrium ordered mechanism with oxygen as the first substrate (eq 3).

Spectra of the His269Ala and His269Gln mutants (Figure 1, curves 3 and 4 respectively) superimpose with the 454 nm band of wild-type enzyme but exhibit a 4 nm hypsochromic shift of the 372 nm band, accompanied by a modest increase in intensity. All of the mutants exhibit values for the extinction coefficient for the bound flavin at 454 nm similar to that for the wild-type enzyme (Table 3). The His269Asn and His269Ala mutants and wild-type MSOX exhibit similar values for the spectral ratio, A_{280}/A_{454}. A modest increase is observed for the His269Gln mutant (Table 3), suggesting a slightly less than stoichiometric incorporation of FAD. The mutant enzymes exhibit specific activity values with sarcosine as substrate that are nearly 2 orders of magnitude lower than observed with wild-type MSOX (Table 3), indicating the importance of His269 in catalysis. The His269Asn mutant was selected for more detailed studies.

Turnover of the His269Asn Mutant with Sarcosine. Double-reciprocal plots of reaction rate *versus* sarcosine concentration at various oxygen concentrations are linear and intersect on the *Y*-axis, as judged by linear regression analysis of data obtained at each oxygen concentration tested (Figure 2A). Double-reciprocal plots of reaction rate *versus* oxygen concentration at various sarcosine concentrations are linear and intersect to the left of the *Y*-axis and above the *X*-axis (Figure 2B). These features are consistent with a rapid equilibrium ordered mechanism with oxygen as the FIRST substrate to bind (Scheme 1). The lines in Figure 2A,B correspond to the global fit of the data to an equation for a rapid equilibrium ordered mechanism (eq 3). In contrast, results obtained for the turnover of wild-type MSOX with sarcosine are consistent with a "modified" ping-pong mechanism where oxygen reacts with the reduced wild-type enzyme prior to the release of the first product (Scheme 2) (*10*). The estimated values for the steady state kinetic parameters obtained for mutant and wild-type enzymes are summarized in Table 4. Turnover of the mutant with sarcosine is nearly 2 orders of magnitude slower than that of the wild type. The K_m values for sarcosine and oxygen are decreased about 2- and 10-fold, respectively, as compared with that for wild-type MSOX.

Scheme 1: Equilibrium Ordered Mechanism with Oxygen as the First Substrate to Bind

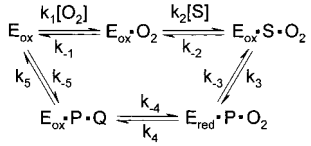

Scheme 2: Modified Ping-Pong Mechanism

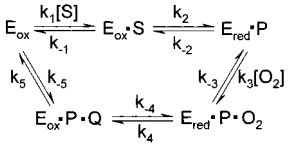

Table 4: Steady-State Kinetic Parameters for the His269Asn Mutant and Wild-Type MSOX with Sarcosine and Oxygen as Substrates

parameter	enzyme: His269Asn	enzyme: wild type[a]
k_{cat} (min^{-1})	110 ± 2	7030 ± 180
$K_{m\ sarcosine}$ (mM)	4.2 ± 0.2	9.4 ± 0.4
$K_{m\ oxygen}$ (mM)	0.034 ± 0.003	0.35 ± 0.02
$K_{d\ sarcosine}$ (mM)		0.6 ± 0.3
mechanism	rapid equilibrium ordered	"modified" ping pong

[a] Data reported by Wagner et al. *(10).*

Reductive Half-Reaction of the His269Asn Mutant with L*-Proline at pH 8.0.* A slow, isosbestic conversion of the oxidized to the fully (two-electron) reduced enzyme is observed upon reaction of the His269Asn mutant with 50 mM L-proline under anaerobic conditions in 100 mM potassium phosphate buffer, pH 8.0, at 4 °C (Figure 3A). The reaction was fully reversible upon aeration. The spectral changes observed with the His269Asn mutant are very similar to that observed for the reaction of wild-type MSOX with 0.21 mM L-proline under otherwise identical conditions (*10*). Formation of an initial E_{ox}•L-proline complex was not detected nor expected in these studies because it was necessary to slow reaction rates by using low substrate concentrations in order to monitor the complete spectral course of the reduction reactions.

The kinetics of the reductive half-reaction at various L-proline concentrations were monitored at pH 8.0 by

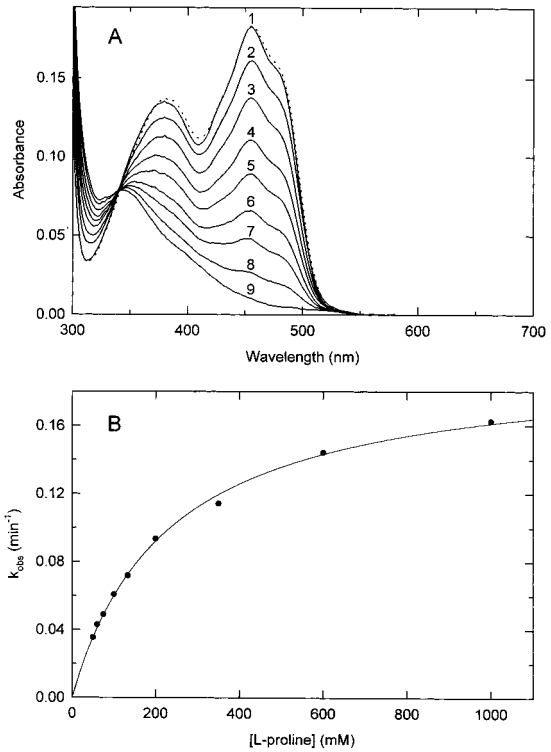

FIGURE 3: Reduction of the His269Asn mutant with L-proline. Reactions were conducted under anaerobic conditions in 100 mM potassium phosphate buffer, pH 8.0, at 4 °C. Panel A: Curves 1−9 (solid lines) were recorded 0, 1.5, 6.0, 13.5, 21.0, 32.0, 45.0, 72.2, and 195.0 min, respectively, after mixing with 50 mM L-proline. The spectrum shown by the dotted line was recorded after air oxidation. Panel B: The observed rate of the anaerobic half-reaction with L-proline is plotted as a function of the substrate concentration. The solid line is a fit of the data to a hyperbolic saturation curve (eq 1).

Scheme 3: Proposed Mechanism for MSOX Reduction by L-Proline

$$\text{E-FAD}_{ox} + \text{S} \underset{}{\overset{K_d}{\rightleftharpoons}} \text{E-FAD}_{ox}\cdot\text{S}$$

$$\text{E-FAD}_{ox}\cdot\text{S} \xrightarrow{k_{lim}} \text{E-FAD}_{red}\cdot\text{P}$$

following the loss of absorbance at 454 nm. The reactions were found to exhibit apparent first-order kinetics over a broad range of L-proline concentrations (0.05−1.0 M). A plot of k_{obs} *versus* L-proline concentration was hyperbolic (Figure 3B). A double-reciprocal plot of the data was linear with a finite *Y*-intercept (not shown). According to criteria described by Strickland et al. (*20*), the data are compatible with the same reductive half-reaction mechanism proposed for wild-type MSOX (Scheme 3). Values for the limiting rate of reduction at saturating L-proline ($k_{lim} = 0.198$ min^{-1}) and the apparent dissociation constant for the E·S complex ($K_d = 230$ mM) were obtained by fitting the data in Figure 3B to eq 1. The His269Asn mutant exhibits a similar binding affinity for L-proline, but the limiting rate of L-proline oxidation at pH 8.0 is decreased by nearly 2 orders of magnitude as compared with that of the wild-type enzyme (Table 5).

Properties of FAD Bound to the His269Asn Mutant. We compared various properties of the flavin in the His269Asn mutant *versus* wild-type MSOX to determine whether the decreased activity observed with sarcosine or L-proline might reflect a significant change in the flavin environment.

Table 5: Reductive Half-Reaction Kinetic Parameters with L-Proline and the His269Asn Mutant or Wild-Type MSOX at pH 8.0[a]

enzyme	k_{lim} (min^{-1})	$K_{L-proline}$ (mM)
His269Asn	0.198 ± 0.004	230 ± 10
wild type	7.4 ± 0.1	260 ± 11

[a] Reductive half-reaction kinetic parameters were determined in 100 mM potassium phosphate buffer, pH 8.0, at 4 °C by fitting the data to eq 1.

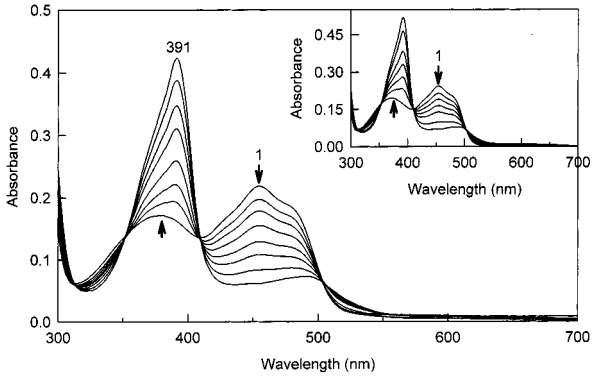

FIGURE 4: Anaerobic reduction of the His269Asn mutant using xanthine/xanthine oxidase as electron donor. Curve 1 is the spectrum of the mutant in anaerobic 50 mM potassium phosphate buffer, pH 8.0, containing 300 μM xanthine, 2 μM methyl viologen, 1 μM 5-deazariboflavin, and 60 μM EDTA, recorded immediately after addition of a catalytic amount of xanthine oxidase at 25 °C. Additional spectra were recorded after 30, 60, 100, 150, 190, 240, and 290 min. Inset: Curve 1 is the spectrum of wild-type MSOX in the same buffer before addition of xanthine oxidase. Additional spectra were recorded 20, 40, *65*, 95, 155, and 230 min after addition of xanthine oxidase. [Reduction of the radical to fully reduced flavin with wild-type or mutant enzyme occurs in a slower reaction (data not shown).]

The pK_a for flavin ionization at N(3) in wild-type MSOX (pK_a = 8.28) (*5*) is shifted downward by 2 pH units as compared with that for free FAD (pK_a = 10.4) (*21*). The absorption spectrum of the His269Asn mutant in the oxidized state is markedly dependent on pH. At pH 7.30 the mutant exhibits absorption maxima at 454 and 377 nm. As the pH is increased from 7.30 to 9.03, the 377 nm peak undergoes an increase in absorbance and a pronounced hypsochromic shift to 368 nm, whereas a decrease in absorbance is observed at 454 nm (data not shown). The spectral changes are very similar to that observed with wild-type MSOX (*5*). Analysis of the absorbance changes observed with the mutant at 352 nm as a function of pH yields a pK_a value of 8.53, similar to that observed with wild-type MSOX.

Wild-type MSOX forms a thermodynamically stable flavin radical in which the anionic form of the radical is stabilized (pK_a < 6 *versus* pK_a = 8.3 with free FAD) (*5*). Reduction of the His269Asn mutant with a xanthine/xanthine oxidase system results in the quantitative formation the anionic radical (Figure 4), similar to observed with wild-type MSOX (Figure 4, inset).

Values for the one-electron potential for the $EFAD_{ox}$/$EFAD^{\bullet-}$ (E_{ox}/E_{rad}) couple (E_1) with the His269Asn mutant or wild-type MSOX were determined using xanthine/xanthine oxidase as reductant with toluylene blue as the indicator dye, according to the method described by Massey (*8*) (Figure 5). The E_1 value obtained for the His269Asn mutant (76.0 mV) is only slightly lower than the value with wild-type

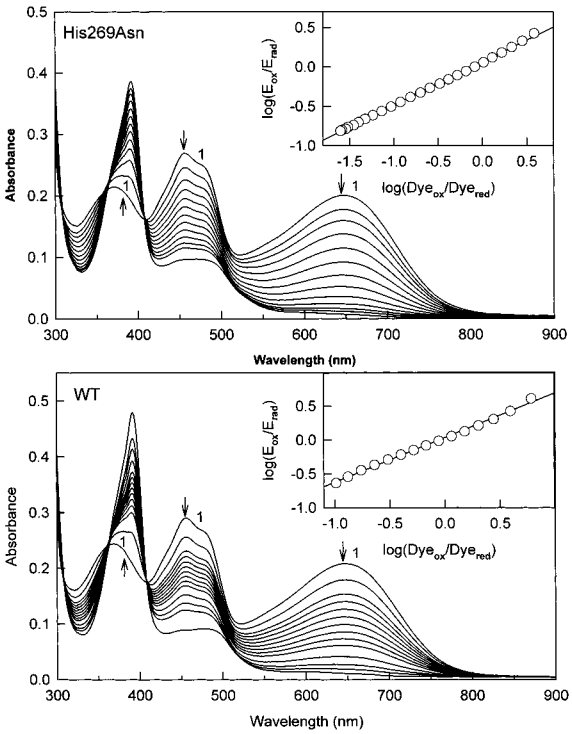

FIGURE 5: Measurement of the one-electron potential for the E_{ox}/E_{rad} couple (E_1) with the His269Asn mutant (top panel) or wild-type MSOX (bottom panel) using toluylene blue as the indicator dye. In each panel, curve 1 is the spectrum of MSOX in anaerobic 50 mM potassium phosphate buffer, pH 8.0, containing 300 μM xanthine, 20 μM methyl viologen, 1 μM 5-deazariboflavin, 60 μM EDTA 300 μM xanthine, and 20 μM toluylene blue at 25 °C. A catalytic amount of xanthine oxidase was tipped from a sidearm. For the His269Asn mutant, additional spectra were recorded after 5, 15, 25, 35, 45, 55, 65, 75, 85, 95, 105, and 155 min. For wild-type enzyme, additional spectra were recorded after 5, 15, 20, 25, 30, 35, 40, 45, 50, 60, 70, 80, and 165 min. Arrows indicate the direction of the spectral change of each absorption band. In each panel, the inset shows a plot of $\log(E_{ox}/E_{rad})$ vs $\log(dye_{ox}/dye_{red})$. Values for the concentration of the oxidized and radical forms of MSOX and the oxidized and reduced forms of toluylene blue were calculated as described in Methods.

Table 6: One-Electron Reduction Potentials of the His269Asn Mutant and Wild-Type MSOX at pH 8.0[a]

enzyme	E_1 (mV)	slope[b]	% radical[c]
His269Asn	76.0 ± 1.7	0.54 ± 0.01	85.3 ± 1.7
wild type	79.5 ± 0.2	0.64 ± 0.02	101.2 ± 2.4

[a] Values are the average of two determinations, using different amounts of xanthine oxidase. [b] The slope is that obtained for a linear plot of $\log(E_{ox}/E_{rad})$ vs $\log(dye_{ox}/dye_{red})$. The theoretical value is 0.5. [c] The amount of radical was estimated using previously determined extinction coefficients for the oxidized and radical forms of wild-type MSOX at 391 nm (5).

enzyme (79.5 mV) (Table 6). These E_1 values are nearly 400 mV more positive than that observed with free flavin (−313 mV) (*22*).

The results show that the His269Asn mutation does not affect the pK_a for flavin ionization, the apparent stability of the anionic radical or the one-electron potential for the E_{ox}/E_{rad} couple.

Structure of His269Asn Mutant. Having established that the properties of the flavin were apparently unaffected by the His269Asn mutation, we proceeded to determine whether the mutation affected the structure of the enzyme. We found

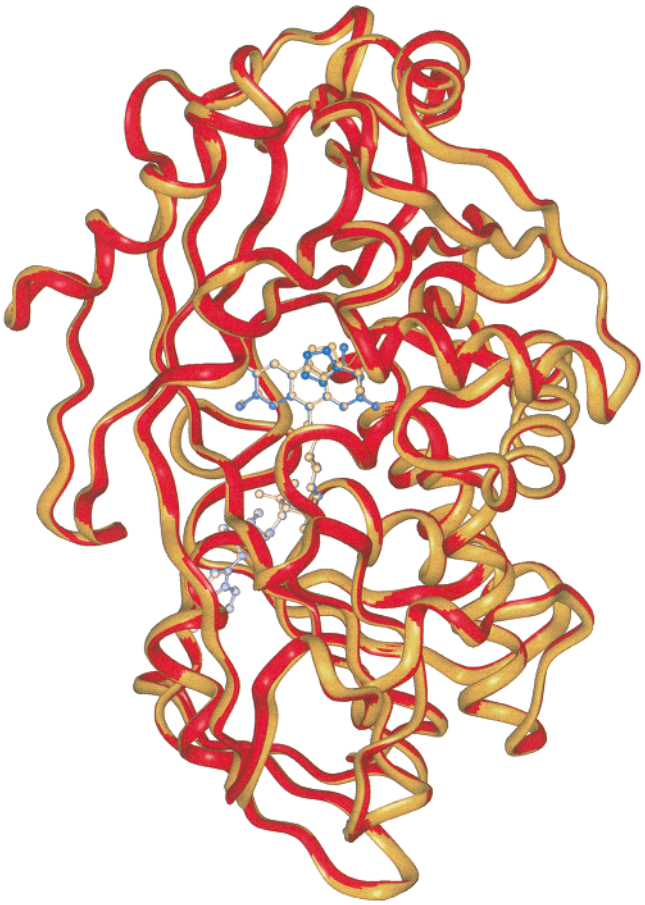

FIGURE 6: Superposition of complexes formed by the His269Asn mutant or wild-type MSOX with a competitive inhibitor, PCA. The protein backbones of mutant and wild-type enzyme are shown by red and gold ribbons, respectively. FAD and inhibitor in mutant (blue) and wild-type enzymes (yellow) are shown by ball-and-stick structures. Comparison is made between subunit 1 in each structure.

in previous studies with wild-type MSOX that the binding of carboxylate-containing ligands (e.g., PCA, MTA) results in the movement of Arg52 into the active site, the displacement of four water molecules that define the substrate binding site in uncomplexed enzyme and the movement of a loop region (Gly56 to Glu60) that forms part of the cleft leading from the surface to the active site. The movement of this loop closes up the active site cleft and prevents additional solvent from accessing the active site (*5*, *6*). Recent studies with a better refined set of coordinates for wild-type MSOX[3] show that the active-site loop in one of the two subunits of ligand-free enzyme is also in the closed configuration, suggesting that the active-site loop is mobile in the absence of substrate and can assume either the open or closed configuration. In the His269Asn mutant, the active-site loop is in the closed configuration in both subunits of ligand-free enzyme (Table 7). Except for this difference, ligand-free wild-type and mutant enzymes exhibit apparently identical structures (data not shown).

The active-site loop remains in the closed configuration upon binding of PCA to the His269Asn mutant. The overall protein conformation of the PCA·complex formed with the mutant enzyme appears to be identical to that of the wild-type enzyme complex (Figure 6). However, small differences in the ligand binding mode are apparent, especially in a close-up view of the active site where the pyrrole ring atoms of

Table 7: Active-Site Loop Configuration in Wild-Type MSOX and the His269Asn Mutant

	free enzyme		PCA complex		imidizole complex	
preparation	subunit 1	subunit 2	subunit 1	subunit 2	subunit 1	subunit 2
wild type	open	closed	closed	closed	1:1, closed/open	closed
His269Asn	closed	closed	closed	closed		

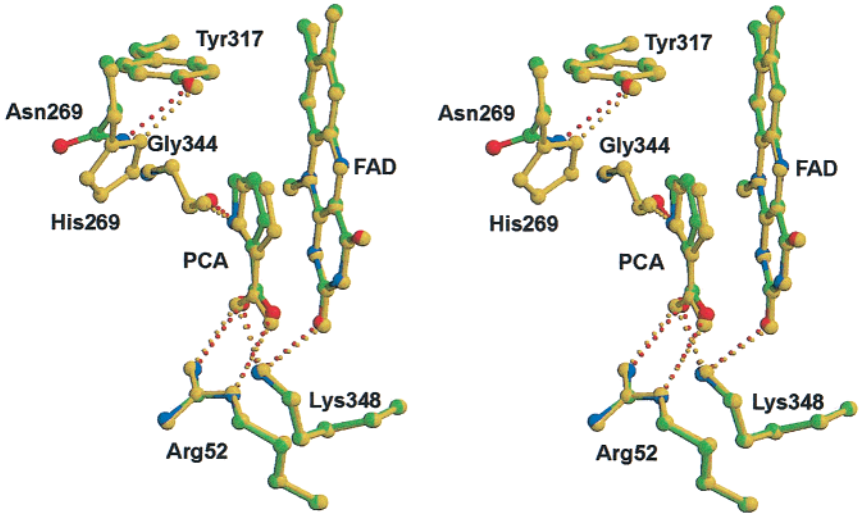

FIGURE 7: Close-up stereoview of the active site in complexes formed by the His269Asn mutant or wild-type enzyme with PCA. The two complexes are superimposed with atoms shown in yellow for wild-type enzyme or in atomic colors for mutant enzyme (C, green; O, red; N, blue). Hydrogen bonds are shown as yellow or red lines for the wild-type or mutant enzymes, respectively. Comparison is made between subunit 1's in each structure.

the inhibitor in the mutant complex are clearly displaced (0.27−0.56 Å) as compared with the wild-type complex (Figure 7). An equivalent set of hydrogen bonds is observed at the active site of the mutant and wild-type complexes with PCA, as illustrated in Figure 7. The distance from O7 to Arg52 NE is, however, longer in the mutant (3.18 and 3.32 Å in subunits 1 and 2, respectively) than in wild-type MSOX (3.00 and 2.98 Å in subunits 1 and 2, respectively), a difference which translates into a somewhat weaker hydrogen bond in the mutant complex. Interestingly, Tyr317 is hydrogen bonded to Asn269 in the mutant. An equivalent hydrogen bond is observed with wild-type enzyme between Tyr317 and His269 ND1.

Complex Formation with Inhibitors and Various His269 Mutants. Could the steric effects leading to the small differences in ligand binding seen with the His269Asn·PCA complex account for the substantial decrease in catalytic activity observed with the mutant enzyme? Overlap of the highest occupied orbital of the donor with the lowest unoccupied orbital of the acceptor is required for electron transfer from substrate to flavin or formation of a charge transfer complex between flavin and a suitable ligand as donor. A mutation that adversely affects the orientation of substrate and ligand orbitals with respect to flavin should therefore decrease catalytic activity and increase the energy of charge-transfer bands, respectively. PCA and methylthioacetate (MTA) are analogues for proline and sarcosine, respectively. Both ligands form charge-transfer complexes with wild-type enzyme (*5*). These ligands also form charge-transfer complexes with the His269Asn mutant, but, significantly, the charge-transfer bands are shifted to shorter wavelengths, and hence higher energy, as compared with wild-type enzyme (Figure 8). A similar effect was also observed for the His269Ala and His269Gln mutants (Table 8).

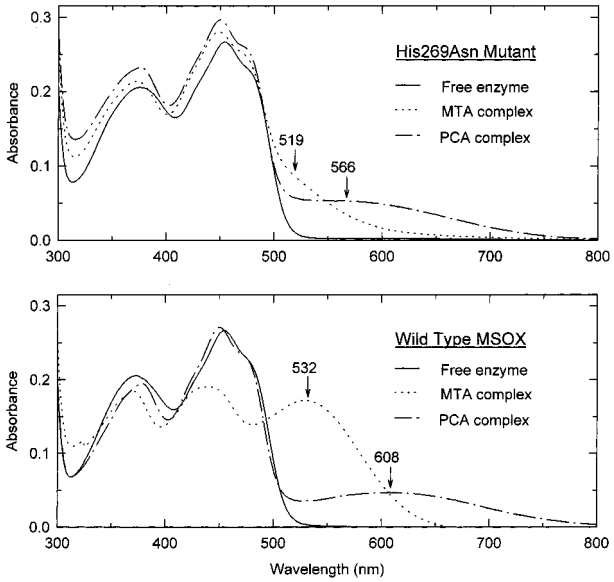

FIGURE 8: Complexes formed with the His269Asn mutant (upper panel) or wild-type MSOX (lower panel) and methylthioacetate (MTA) or pyrrole-2-carboxylate (PCA) In each panel, the solid line shows the absorption spectrum of the free enzyme in 50 mM potassium phosphate buffer, pH 8.0, at 25 °C. Spectra of complexes with MTA and PCA (dotted and dash−dot lines, respectively) are normalized to 100% complex formation, as described in Experimental Procedures. The data for the all complexes are also normalized to the same initial enzyme concentration (A_{454} = 0.27). The positions of charge-transfer bands were estimated on the basis of maxima observed in difference spectra (not shown).

Spectral Properties of the E_{ox}·S Complex Formed with the His269Asn Mutant and L-Proline at pH 8.0. The results described above are consistent with the possibility that

Table 8: Complexes Formed with Inhibitors and Various His269 Mutants[a]

ligand	enzyme	K_d (mM)	Charge Transfer Band λ_{max} (nm)	Charge Transfer Band ϵ ($mM^{-1}cm^{-1}$)
methylthioacetate	wild type	2.88	532	7.7
	His269Ala	25.4	522	2.4
	His269Asn	14.2	519	2.0
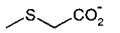	His269Gln	122	520	3.2
pyrrole-2-carboxylate	wild type	1.60	608	2.0
	His269Ala	70.0	540	1.9
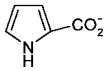	His269Asn	39.9	566	1.4

[a] Complexes were formed in 50 mM potassium phosphate buffer, pH 8.0, at 25 °C.

His269 plays an important role in optimizing ligand/substrate binding but do not address the possibility that His269 might be the active-site residue with a pK_a of 8.0, a feature which might also contribute to the decreased activity observed with the His269 mutants. In an initial attempt to address this issue, we examined the spectral properties of the E·S complex formed with the His269Asn mutant and L-proline. The absolute spectrum of this complex at pH 8.0 does not exhibit a new band at longer wavelengths (Figure 9A), unlike wild-type MSOX (see accompanying paper). The difference spectrum exhibits a peak at 502 nm (Figure 9B) which might reflect the 2 nm bathochromic shift of the 454 nm band rather than a charge-transfer interaction. We considered two possible reasons for the failure to observe a definitive charge-transfer band with the mutant enzyme·L-proline complex. (1) His269 is the active-site base required for conversion of the zwitterionic substrate to the anionic form that can act as a charge transfer donor. (2) His269 is not the active-site base. A charge-transfer complex is formed with the L-proline anion. Unlike PCA and MTA, the charge-transfer band with the mutant enzyme·L-proline complex is difficult to detect because the charge-transfer band with the wild-type enzyme·L-proline complex absorbs at shorter wavelengths (512 nm *versus* 608 or 532 nm with PCA or MTA, respectively). A similar increase in the energy of the charge-transfer band with the His269Asn·L-proline complex might cause the charge-transfer band to be hidden under the red edge of the flavin absorption band. Thus, the data obtained with MTA or PCA predict a charge-transfer band for the L-proline·mutant complex with a maximum at 500 or 482 nm, respectively. A charge-transfer band of modest intensity at these wavelengths might be difficult to detect.

Effect of pH on the Spectral Properties of the E_{ox}·S Complex Formed with the His269Asn Mutant and L-Proline. The absorption spectrum of the His269Asn mutant was recorded before and immediately after mixing with 600 mM L-proline in aerobic buffers at pH ≤ 9.0, a pH range where observed values for K_d are pH-independent (K_d = 228 mM, *vide infra*). Under these conditions most of the mutant enzyme is converted to the E_{ox}·S complex. Although the dissociation constant of the E_{ox}·S complex is pH-independent,

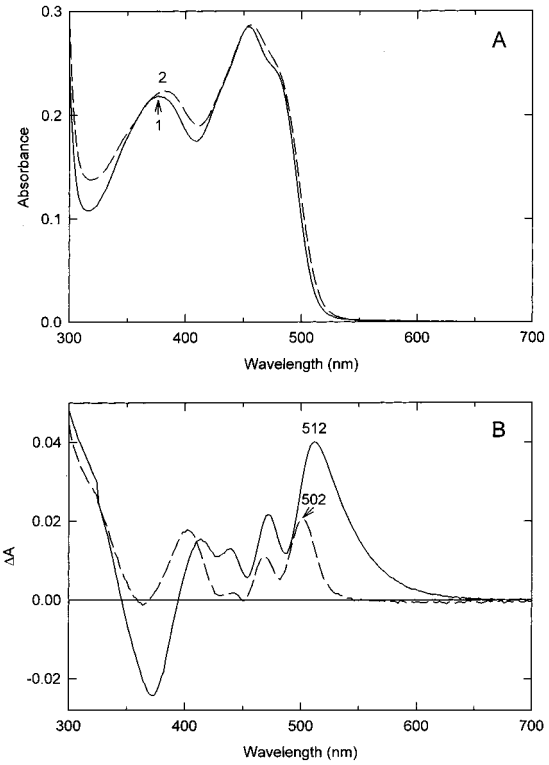

FIGURE 9: Complex formed with L-proline and the His269Asn mutant. Panel A shows absolute absorption spectra. Curve 1 (solid line) is the free His269Asn mutant enzyme in aerobic 50 mM potassium phosphate buffer, pH 8.0, at 4 °C. Curve 2 (dashed line) was recorded immediately after addition of 600 mM L-proline. Enzyme reduction was observed when the dissolved oxygen was consumed by turnover (data not shown). Panel B shows difference spectra for mutant enzyme (dashed line) and wild-type MSOX (solid line). The data for the wild-type and mutant enzyme are normalized to the same initial enzyme concentration.

the observed perturbation of the absorption spectrum was found to be pH-dependent (Figure 10A). The mutant enzyme results are similar to those of the wild-type enzyme (see accompanying paper) except for the hypsochromic shift in maxima seen in the respective difference spectra. A pK_a value of 8.12 was obtained for the mutant enzyme by fitting the absorbance increase at 502 nm to a theoretical pH titration curve (Figure 10b). The observed pK_a is very similar to the value obtained observed in a similar experiment with wild-type MSOX (pK_a = 7.94).

Effect of pH on the Reductive Half-Reaction of the His269Asn Mutant with L-proline. The effect of pH on the reductive half-reaction of the His269Asn mutant with L-proline was studied in the pH range 7.5−9.4. The lower pH range was limited by the instability of the mutant enzyme and slow reaction rates at acidic pH values. As indicated above, the observed values for K_d were pH-independent in the range from pH 7.5−9.0 (K_d = 228 ± 6.9 mM), similar to wild-type MSOX (K_d = 256 ± 4 mM). [A decrease in K_d was observed with the His269Asn mutant at higher pH values (K_d = 181.9 and 171.4 mM at pH 9.2 and 9.4, respectively)]. The values for k_{lim} with the mutant were strongly pH-dependent. The rates decreased at low pH, similar to wild-type MSOX, but did not reach a plateau at pH 9.0 (Figure 11), unlike wild-type, enzyme (see accompanying paper). Instead, values for k_{lim} with the mutant enzyme exhibit a decrease at pH > 9. The data for the mutant enzyme were

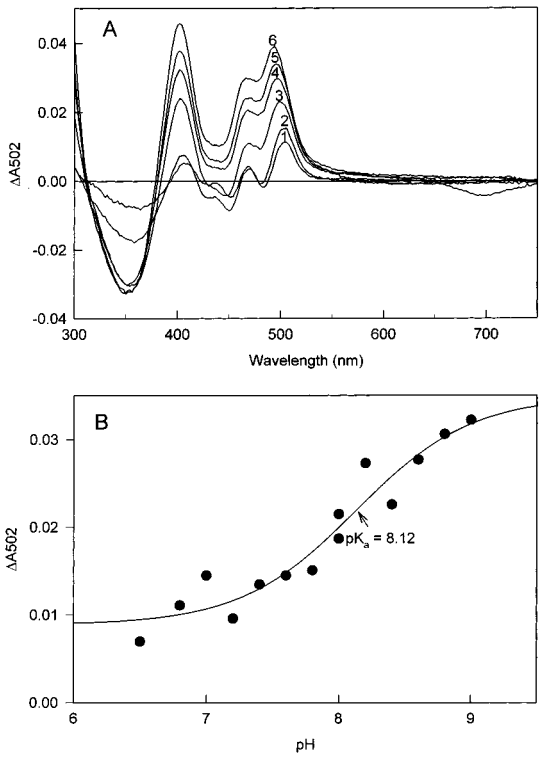

FIGURE 10: Effect of pH on the spectral perturbation observed upon complex formation with the His269Asn mutant and L-proline. Panel A: Spectra were recorded before and immediately after mixing the His269Asn mutant (20.0 μM) with 600 mM L-proline. Reactions were conducted under aerobic conditions in 100 mM potassium phosphate buffer (pH $\leq$ 8.0) or potassium pyrophosphate buffer (pH $\geq$ 8.0) at 4 °C. Curves 1−6 are difference spectra obtained for reactions at pH 9.0, 8.8, 8.6, 8.4, 7.8, and 6.8, respectively. Panel B: The observed difference in absorption at 502 nm is plotted as a function of pH (closed circles). The solid line is a fit of the data to eq 2.

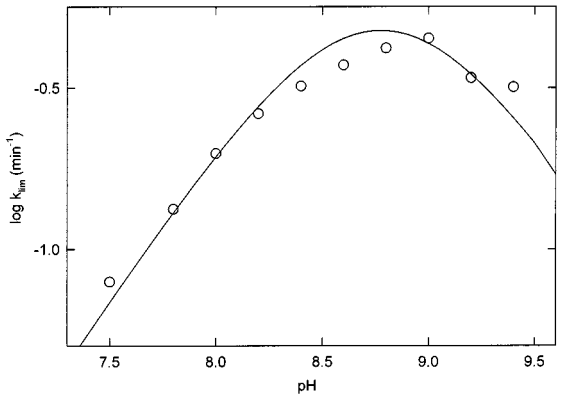

FIGURE 11: Effect of pH on the limiting rate of reduction (k_{lim}) of the His269Asn mutant enzyme at saturating L-proline. Reactions were conducted under anaerobic conditions in 100 mM potassium phosphate buffer (pH $\leq$ 8.0) or potassium pyrophosphate buffer (pH $\geq$ 8.0) at 4 °C. Values for k_{lim} were obtained by fitting the observed rates a various L-proline concentrations to eq 1. The solid line is a fit of the data (open circles) to eq 4.

best fitted by eq 4, where K_{a1} is the apparent ionization constant of a group in the E·S complex that must be unprotonated for enzyme reduction to occur (pK_{a1} = 8.85) and K_{a2} is the *apparent* ionization constant of a group in the E·S complex that must be protonated for enzyme reduction to occur (pK_{a2} = 8.70). It should be emphasized that only apparent pK_a values are obtained by fitting the data to eq 4

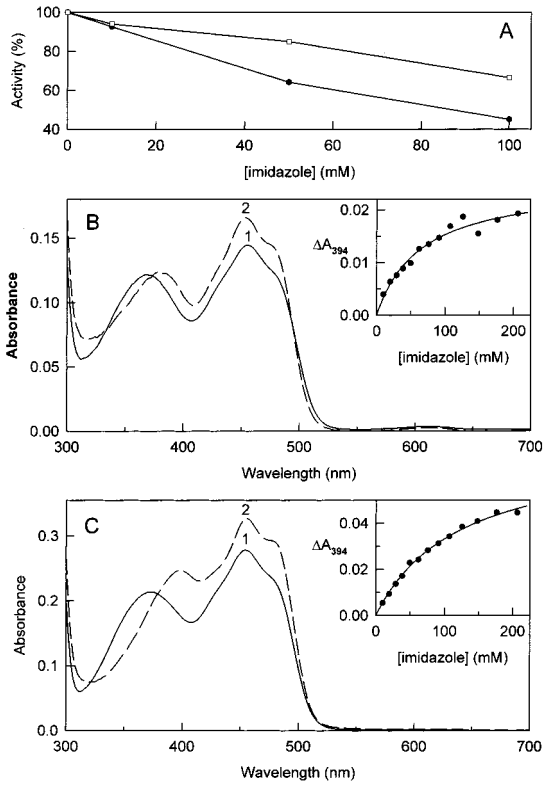

FIGURE 12: Binding of imidazole to the His269Ala mutant and wild-type enzyme. Panel A shows the inhibition of wild-type MSOX (open squares) and the His269Ala mutant (solid circles) in the presence of various concentrations of imidazole. Reactions were conducted using the standard horseradish peroxidase assay (10), except that the sarcosine concentration was reduced from 120 mM to 5 mM. Panels B and C show the effect of imidazole on the absorption spectrum of the His269Ala mutant and wild-type MSOX, respectively. In each case, curve 1 is the absorption spectrum of the free enzyme in 50 mM potassium phosphate buffer, pH 8, at 25 °C, and curve 2 is the spectrum of the imidazole complex, normalized to 100% complex formation, as described in Experimental Procedures. The insets show plots of the observed absorbance increases at 394 nm. The solid lines are fits of the data to a theoretical binding curve (eq 1).

in the case where pK_{a2} − pK_{a1} < 0.6. The average of the two pK_a's (p$K_{a\ (average)}$ = 8.78) is accurately determined, but not the individual pK_a values, because the fit to eq 4 is degenerate when pK_{a2} − pK_{a1} < 0.6 (*23*). A true value for pK_{a1} is, however, provided by the pK_a obtained from spectral titration of the mutant enzyme·L-proline complex (pK_a = 8.12) (see Figure 10). A true value for pK_{a2} can therefore be calculated (pK_{a2} = 9.43) using the true value for pK_{a1} and the average of pK_{a1} and pK_{a2} obtained from the fit of the reductive-half reaction data to eq 4. The pK_a of the group in the mutant enzyme E·S complex which must be protonated is significantly perturbed by mutation of His269 since no evidence for a second ionizable group was observed with wild-type MSOX in reductive half-reaction studies with L-proline up to a pH value of 9.4. The results indicate that His269 is not the active-site base with a pK_a of 8.0 since the same ionizable group is observed in the E·S complex-formed L-proline and the His269Asn mutant or wild-type MSOX.

Attempted Chemical Rescue of the His269Ala Mutant. Previous studies in other systems have shown that mutants exhibiting decreased catalytic activity owing to the loss of an important active-site base can be rescued by addition of a small base such as imidazole (*24*). Since His269 can be

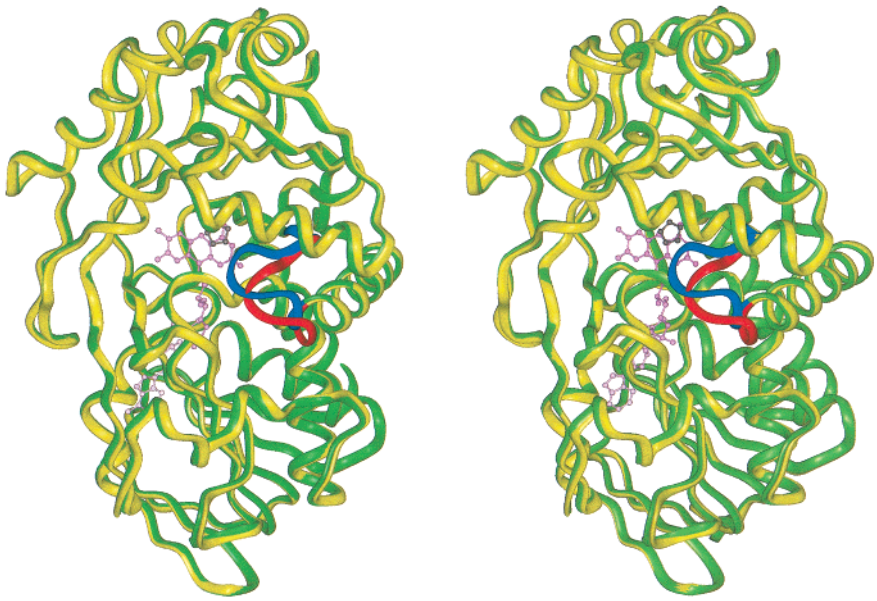

FIGURE 13: Stereo ribbon diagrams of the imidazole complex with wild-type MSOX. FAD (pink) and imidazole (grey) are shown as ball-and-stick models. There are two MSOX molecules in the asymmetric unit. One molecule is entirely in the active-site-closed conformation, whereas the other is a 1:1 mix of open and closed conformations. Molecules with the active-site loop in the closed (blue) or open (red) conformation are otherwise superimposable, as shown by the green and yellow ribbons, respectively.

Table 9: Complexes Formed with Imidazole and Wild-Type MSOX or the His269Ala Mutant[a]

	K_d (mM)	
pH	wild type	His269Ala
7.0	301 ± 10	
8.0	121 ± 9	64 ± 11
8.5	126 ± 9	

[a] Measurements were conducted in 50 mM potassium phosphate buffer (pH 7 and 8) or 50 mM Tris buffer (pH 8.5) at 25 °C.

excluded as the active-site base in MSOX, we expected that addition of imidazole would have little effect on the activity of the His269Ala mutant. Surprisingly, imidazole actually inhibited sarcosine oxidation by the His269Ala mutant. Additional studies, however, showed that wild-type enzyme was also inhibited by imidazole (Figure 12A) and that both mutant and wild-type enzyme formed spectrally detectable complexes with imidazole (Figure 12B,C). The binding of imidazole to the mutant enzyme at pH 8.0 is 2-fold tighter than that of wild-type enzyme (Table 9). Studies with wild-type MSOX suggest that the enzyme binds the unprotonated form of imidazole ($pK_a = 7.05$), as judged by the pH-dependence of the observed dissociation constant (Table 9).

Crystal Structure of the Complex of Imidazole with Wild-Type MSOX. Crystals of the complex of wild-type MSOX with imidazole contain two enzyme molecules (subunits) in the asymmetric unit, as previously observed for free wild-type MSOX and its complexes with other inhibitors (*5*, *6*). One molecule in the MSOX·imidazole complex is in the active-site-closed conformation, whereas the other is a 1:1 mix of open and closed conformations. In contrast, the active-site loop is entirely in the closed conformation for complexes of wild-type MSOX and other inhibitors (Table 7) (*5*, *6*). Except for the active-site loop and the location of Arg52, the two conformations of the MSOX·imidazole complexes are otherwise superimposable (Figure 13). Figure 14 (top panel) shows a close-up view of the imidazole complex in the active-site-closed conformation where Arg52 has moved into the active site. Imidazole is bound parallel to and 3.65 Å above the pyrimidine subnucleus of the flavin ring. The binding of imidazole results in the displacement of *three* of the *four* active-site water molecules that are displaced by other inhibitors. The fourth water is retained in the imidazole complex and is hydrogen bonded to N(3) of the inhibitor (2.78 Å), the carbonyl oxygen of Gly344 (2.71 Å), and the phenolic oxygen of Tyr317 (2.68 Å). Imidazole N(1) is hydrogen bonded to Arg52 NH_2 (2.95 Å) and Lys348 NZ (3.08 Å). In the PCA complex, Arg52 and Lys348 are hydrogen bonded to the carboxylate oxygens of the ligand. The imidazole and PCA complexes of wild-type MSOX are compared in the bottom panel of Figure 14. In the PCA complex, the ligand is bound somewhat closer to the flavin ring (3.3 Å) than in the imidazole complex (3.65 Å). The carbonyl oxygen of Gly344 directly participates in PCA binding via a hydrogen bond to the pyrrole nitrogen, in contrast to the imidazole complex where the interaction is indirect and mediated by the bridging water molecule. As compared with the pyrrole ring of PCA, the imidazole ring is shifted toward the pyrimidine subnucleus of the flavin and partially overlaps with the carboxylate moiety of PCA. Except for the retained water molecule and the ligands themselves, the active sites in the imidazole and PCA complexes are virtually superimposable.

DISCUSSION

Mutation of His269 to Asn, Ala, or Gln does not significantly affect MSOX expression, covalent flavinylation, or the visible absorption spectrum of the isolated enzyme. The specific activity of the each mutant enzyme is, however, decreased by nearly 2 orders of magnitude as compared with wild-type MSOX, indicating the importance of His269 in MSOX catalysis. Additional studies with the His269Asn mutant show that mutation of His269 does not affect the pK_a for flavin ionization at N(3), the stability of the anionic radical, or the one-electron potential for the E_{ox}/E_{rad} couple.

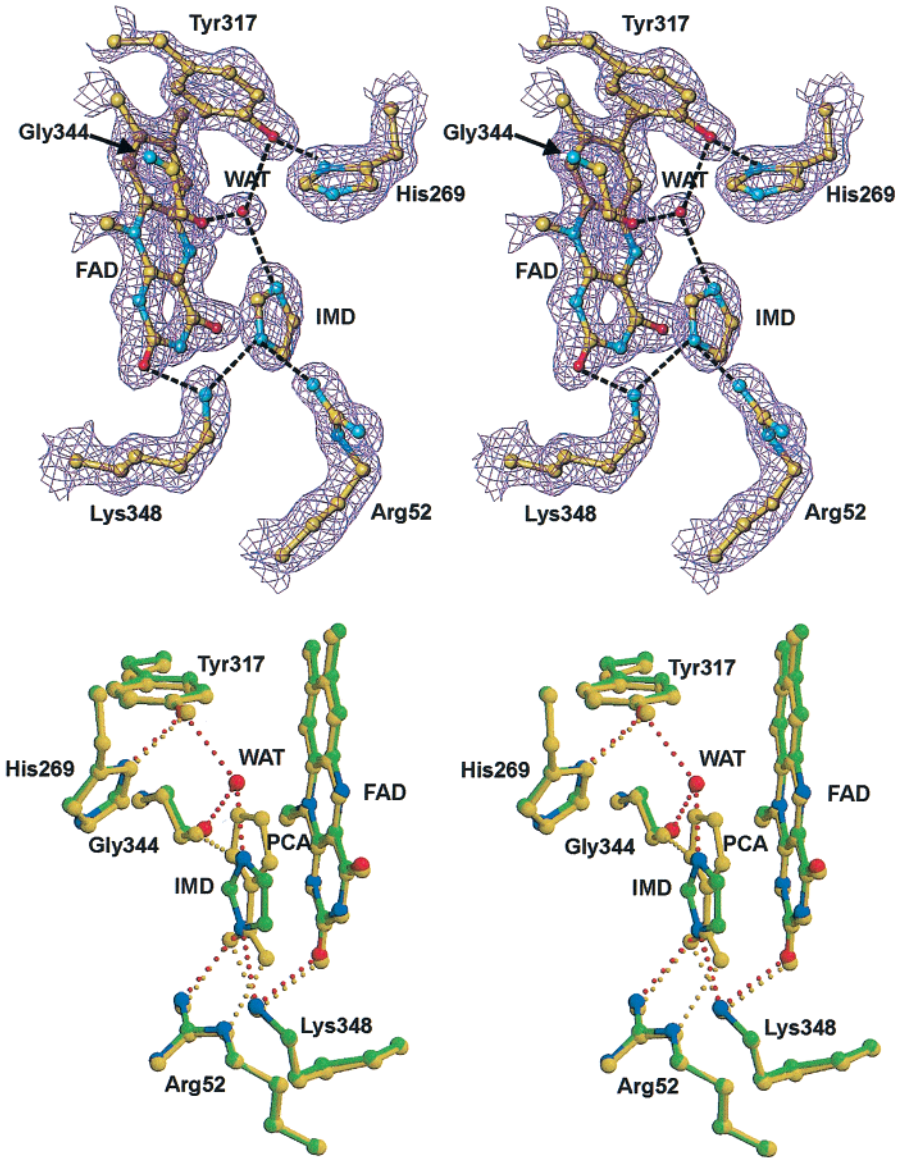

FIGURE 14: Binding of imidazole to wild-type MSOX. The imidazole complex is shown in the active-site-closed conformation. The top panel shows a stereoview of the 2Fo−Fc electron density map of the MSOX·imidazole complex. A ball-and-stick representation for imidazole, the flavin ring, and several interacting side and main chain atoms is included. The contour level is 1.0 σ. The atom colors are carbon (gold), nitrogen (cyan), and oxygen (red). Hydrogen bonds are shown as black dotted lines. In the bottom panel, stereo diagrams of the wild-type MSOX complexes with imidazole and PCA are superimposed. The atom colors for the imidazole complex are carbon (green), nitrogen (blue), and oxygen (red). All atoms in the PCA complex are colored yellow. Hydrogen bonds for the imidazole and PCA complexes are shown as red and yellow dotted lines, respectively.

The results suggest that His269 is present in an unprotonated form in wild-type MSOX since the loss of a nearby positive charge might otherwise be expected to effect both N(3) ionization and the one-electron reduction potential of the flavin (*25*, *26*).

To characterize the nature of the catalytic impairment, we conducted steady-state and reductive half-reaction studies with the His269Asn mutant. Turnover with sarcosine at pH 8.0 is nearly 2 orders of magnitude slower than that with wild-type MSOX. The mutant data are consistent with a rapid equilibrium ordered mechanism with oxygen as the first substrate to bind (Scheme 1), whereas a modified ping-pong mechanism is observed for wild-type MSOX (Scheme 2). The basis for this change in steady-state mechanism is unclear. The same change in mechanism is, however, observed with wild-type *N*-methyltryptophan oxidase (a member of the MSOX family) when *N*-methyltryptophan is replaced by sarcosine, a poor substrate for this enzyme (*27*). The effect of the His269Asn mutation on the MSOX reductive half-reaction was evaluated in studies with L-proline at pH 8.0, which show that the mutation decreases the limiting rate of reduction (k_{lim}) by nearly 2 orders of magnitude whereas the K_d for formation of the E_{ox}·S complex is unaffected. Reduction of the mutant enzyme by L-proline involves rapid equilibration of free enzyme with the E_{ox}·S complex, followed by a practically irreversible reduction of the enzyme flavin to form E_{red}·P (Scheme 3). The same mechanism is observed with wild-type MSOX.

The crystal structure of the free His269Asn mutant and the complex of the mutant enzyme with PCA show that the mutation does not affect the overall structure of MSOX. PCA bound to the mutant enzyme does not, however, completely superimpose with PCA bound to wild-type MSOX. Small differences are observed, especially in the orientation of the

pyrrole ring of the inhibitor which is displaced by 0.27−0.56 Å in the mutant enzyme as compared with wild-type MSOX. The three His269 mutants (His269Asn, His269Ala, His269Gln) form charge-transfer complexes with PCA and MTA, inhibitors that are analogues for L-proline and sarcosine substrates, respectively. The charge-transfer bands with the mutant enzymes are, however, shifted to shorter wavelengths, and hence higher energy, as compared with wild-type MSOX. A decrease in the one-electron potential for the E_{ox}/E_{rad} couple (E_1) with the His269 mutants as compared with wild-type MSOX might account for the observed hypsochromic shift of the charge-transfer bands, but this explanation can be ruled out because similar E_1 values are observed with His269Asn mutant (76.0 ± 1.7 mV) and wild-type (79.5 ± 0.2 mV) enzymes. Charge and electron transfer reactions can also be affected by the environment, but the His269Asn mutant and wild-type enzyme exhibit similar active-site environments, as judged by structural data and the properties observed for the FAD prosthetic group. We propose that the increased energy of the charge transfer-bands observed with the mutant complexes is due to a change in ligand orientation, resulting in a less than optimal overlap of the highest occupied orbital of the ligand with the lowest unoccupied orbital of the flavin. A similar alteration in substrate orientation might decrease the rate of electron transfer and might thereby account for the nearly 100-fold decrease in reaction rates observed with the mutant enzyme.

The binding of L-proline to wild-type MSOX and the His269Asn mutant is pH-independent at pH ≤ 9.0, indicating that both enzymes bind the zwitterionic form of L-proline from solution. The absorption spectrum of the E_{ox}·S complex formed with the His269Asn mutant does not provide evidence for charge-transfer interaction, even at elevated pH and L-proline concentrations (1,000 mM L-proline, pH 10.0), unlike wild-type MSOX (see accompanying paper). Charge-transfer complex formation with wild-type MSOX exhibits a pK_a = 8.0 and requires conversion of enzyme-bound L-proline from the zwitterionic to the anionic form. Significantly, the spectral perturbation observed for the His269Asn·L-proline complex is also pH-dependent, exhibiting a pK_a value of 8.1, similar to that observed for the development of the charge-transfer band with wild-type enzyme. The results indicate that His269 is not the ionizable group (pK_a = 8.0) associated with charge-transfer complex formation with wild-type MSOX and L-proline. We postulate that a charge transfer complex is actually formed with L-proline and the mutant enzyme but, unlike PCA and MTA, the charge-transfer band with the mutant enzyme·L-proline complex is difficult to detect. This difference arises because the charge-transfer band with the wild-type enzyme·L-proline complex absorbs at shorter wavelengths (512 nm) as compared with the PCA (608 nm) or MTA (532 nm) complexes. A similar increase in the energy of the charge-transfer band with the His269Asn·L-proline complex might, therefore, cause the charge-transfer band to be hidden under the red edge of the flavin absorption band. Analysis of the effect of pH on the limiting rate of reduction of the His269Asn mutant indicates that an ionizable group in the E_{ox}·S complex with a pK_a = 8.0 must also be unprotonated for conversion of E_{ox}·S to E_{red}·P whereas a second group with a pK_a = 9.4 must be protonated. The latter group is not detected with wild-type enzyme, suggesting that its pK_a is decreased upon mutation of His269.

The results clearly indicate that His269 is not the group with a pK_a = 8.0 that must be unprotonated for conversion of L-proline to the reactive anionic form that undergoes electron transfer to FAD. This leaves L-proline or Tyr317 as potential candidates for the ionizable group in the E·S complex. Tyr317 mutagenesis studies with MSOX are currently in progress. If the pH effect is not eliminated by mutation of Tyr317, the results would indicate that the MSOX active site causes a substantial lowering of the pK_a of L-proline as compared with the free ligand (pK_a = 10.6). A similar shift in the substrate pK_a is observed upon binding of trimethylamine to trimethylamine dehydrogenase (pK_a = 6.5 for E_{ox}·S vs pK_a = 9.3 with free S) (*28*, *29*).

Since His269 could be ruled out as the active-site base in the E·S complex with L-proline, we expected that the His269Ala mutant would not be subject to chemical rescue. Addition of a small base like imidazole was, therefore, not expected to affect enzyme activity. Instead, we found that imidazole was an inhibitor that bound to the active site in both mutant and wild-type enzyme. The binding of imidazole to wild-type MSOX was completely unexpected. Our previous studies led us to conclude that the carboxylate moiety of sarcosine ($CH_3NHCH_2\mathbf{CO_2^-}$) was essential for binding of ligands, in part, because no binding was observed with simple aliphatic amines such as ethylmethylamine (CH_3-$NHCH_2\mathbf{CH_3}$). Interestingly, our results indicate that MSOX probably binds the *unprotonated* form of imidazole. This suggests that one reason aliphatic amines do not bind to MSOX is because they are *protonated* at neutral pH (pK_a > 10). The ability to bind imidazole provides insight into the plasticity of the MSOX active site. Imidazole N(1) forms hydrogen bonds with Arg52 and Lys348, residues that "normally" bind the carboxylate group of substrate and substrate analogues. Imidazole also forms a hydrogen bond with a water molecule that is displaced upon binding of carboxyl-containing ligands. The imidazole binding site is shifted toward the pyrimidine subnucleus of the flavin, as compared with carboxyl-containing ligands, a feature which may favor aromatic stacking interactions and thus contribute to imidazole binding energy.

ACKNOWLEDGMENT

We thank Peeyush Khana for initial work on the redox potentials of MSOX. We thank Russ Hille for his generous gift of xanthine oxidase. We thank Drs. Paul Fitzpatrick and John Schloss for helpful discussions.

REFERENCES

1. Wagner, M. A., Khanna, P., and Jorns, M. S. (1999) *Biochemistry 38*, 5588−5595.
2. Kvalnes-Krick, K. and Jorns, M. S. (1991) in *Chemistry and Biochemistry of Flavoenzymes* (Muller, F., Ed.) pp 425−435, CRC Press, Inc., Boca Raton, FL.
3. Chlumsky, L. J., Zhang, L., and Jorns, M. S. (1995) *J. Biol. Chem. 270*, 18252−18259.
4. Reuber, B. E., Karl, C., Reimann, S. A., Mihalik, S. J., and Dodt, G. (1997) *J. Biol. Chem. 272*, 6766−6776.
5. Wagner, M. A., Trickey, P., Chen, Z., Mathews, F. S., and Jorns, M. S. (2000) *Biochemistry 39*, 8813−8824.
6. Trickey, P., Wagner, M. A., Jorns, M. S., and Mathews, F. S. (1999) *Structure 7*, 331−345.

7. Ho, S. N., Hunt, H. D., Horton, R. M., Pullen, J. K., and Pease, L. R. (1989) *Gene 77*, 51−59.
8. Massey, V. (1991) in *Flavins and Flavoproteins* (Curti, B., Ronchi, S., and Zanetti, G., Eds.) pp 59−66, de Gruyter, Berlin.
9. Clark, W. M. (1960) *Oxidation-Reduction Potential of Organic Systems* The Williams and Wilkins Co., Baltimore.
10. Wagner, M. A. and Jorns, M. S. (2000) *Biochemistry 39*, 8825−8829.
11. Otwinowski, Z. and Minor, W. (1997) *Methods Enzymol. 276*, 307−326.
12. Navaza, J. (1994) *Acta Crystallogr., Sect. A 50*, 157−163.
13. Brünger, A. T., Adams, P. D., Clore, G. M., DeLano, W. L., Gros, P., Grosse-Kunstleve, R. W., Jiang, J. S., Kuszewski, J., Nilges, M., Pannu, N. S., Read, R. J., Rice, L. M., Simonson, T., and Warren, G. L. (1998) *Acta Crystallogr., Sect. D 54*, 905−921.
14. Kleywegt, G. J.; Brünger, A. T. (1996) *Structure 4*, 897−904.
15. Jiang, J.-S.; Brüinger, A. T. (1994) *J. Mol. Biol. 243*, 100−115.
16. Allen, F. H., and Kennard, O. (1993) *Chem. Design Automation News 8*, 1−31.
17. Roussel, A., and Cambillau, C. (1991) in *Silicon Graphics Geometry Partners Directory 86* Silicon Graphics, Mountain View, CA.
18. Ramachandran, G. N, and Sasisekharan, V. (1968) *Adv. Protein Chem. 23*, 283−438.
19. Laskowski, R. A., MacArthur, M. W., Moss, D. S., and Thornton, J. M. (1993) *J. App. Cryst. 26*, 283−291.
20. Strickland, S., Palmer, G., and Massey, V. (1975) *J. Biol. Chem. 250*, 4048−4052.
21. Massey, V, and Ganther, H. (1965) *Biochemistry 4*, 1161−1173.
22. Mayhew, S. G. (1999) *Eur. J. Biochem. 265*, 698−702.
23. Cleland, W. W. (1977) *Adv. Enzymol. 45*, 273−387.
24. Toney, M. D, and Kirsch, J. F. (1989) *Science 243*, 1485−1488.
25. Zhou, Z. M, and Swenson, R. P. (1995) *Biochemistry 34*, 3183−3192.
26. Swenson, R. P, and Zhou, Z. (1997) in *Flavins and Flavoproteins 1996* (Stevenson, K. J., Massey, V., and Williams, C. H. J., Eds.) pp 427−436, University of Calgary Press, Calgary.
27. Khanna, P, and Jorns, M. S. (2001) *Biochemistry 40*, 1441−1450.
28. Basran, J., Sutcliffe, M. J., and Scrutton, N. S. (2001) *J. Biol. Chem. 276*, 42887−42892.
29. Basran, J., Sutcliffe, M. J., and Scrutton, N. S. (2001) *J. Biol. Chem. 276*, 24581−24587.

BI020286F